A&A 469, 587–593 (2007)
DOI: 10.1051/0004-6361:20066206

Astronomy & Astrophysics

Resolving the B[e] star Hen 3-1191 at 10 μm with VLTI/MIDI⋆

R. Lachaume[1,2], Th. Preibisch[2], Th. Driebe[2], and G. Weigelt[2]

[1] Centro de Radioastronomía y Astrofísica UNAM, Apartado Postal 3-72 (Xangari), Morelia, CP 58089 Michoacán, Mexico
e-mail: r.lachaume@astrosmo.unam.mx
[2] Max-Planck-Institut für Radioastronomie, Auf dem Hügel 69, 53121 Bonn, Germany

Received 7 August 2006 / Accepted 28 March 2007

ABSTRACT

We report spatially resolved, spectrally dispersed N-band observations of the B[e] star Hen 3-1191 with the MIDI instrument of the Very Large Telescope Interferometer. The object is resolved with a 40 m baseline and has an equivalent uniform disc diameter ranging from 24 mas at 8 μm to 36 mas at 13 μm. The MIDI spectrum and visibilities show a curvature which can arise from a weak silicate feature in which the object appears ≈15% larger than in the continuum, but this could result from a change in the object's geometry within the band.

We then model Hen's 3-1191 spectral energy distribution (.4−60 μm) and N-band visibilities. Because of the unknown nature of the object, we use a wide variety of models for objects with IR excesses. We find the observations to be consistent with a disc featuring an unusually high mass accretion and a large central gap almost void of matter, an excretion disc, and a binary made of two IR sources. We are unable to find a circumstellar shell model consistent with the data.

We review the different hypotheses concerning the physical nature of the star and conclude that it is neither a Be supergiant nor a symbiotic star. However, we could not discriminate between the scenario of a young stellar object featuring an unusually strong FU Orionis-like outburst of mass accretion ($4–250\times10^{-4}$ $M_\odot$/yr) and that of a protoplanetary nebula with an equatorial mass excretion rate $\gtrsim 4 \times 10^{-5}$ $M_\odot$/yr. In both cases, taking the additional presence of an envelope or wind into account would result in lower mass flows.

Key words. stars: emission-line, Be – stars: individual: Hen 3-1191 – planetary systems: protoplanetary disks – infrared: stars – accretion, accretion disks – technique: interferometric

1. Introduction

Hen 3-1191 ($\alpha = 16^h27^m15''$, $\delta = -48°39'27''$, $V = 13.7$), also known as WRAY 15-1484, SS73 56 or VRMF 31, is a member of the B[e] spectral class as defined by Allen & Swings (1972, 1976); Lamers et al. (1998). It features:

- strong Balmer emission lines;
- low-excitation permitted emission lines of low-ionisation metals in the optical;
- forbidden emission lines of [Fe II] and [O I] in the optical, evidence for a diffuse circumstellar (CS) environment;
- a strong near or mid-infrared excess hinting towards hot CS dust.

A review of the properties of these still mysterious emission-line stars was given by Zickgraf (1998).

Though these properties indicate similar physical conditions in the CS environment of B[e] stars in terms of temperature, density, and velocity, these stars form a highly heterogeneous group. As categorised by Lamers et al. (1998), they comprise various objects : B[e] supergiants (sgB[e]), young stellar objects (YSOs) of Herbig type (HAeB[e]), compact planetary nebulae (cPNB[e]), and symbiotic stars (symB[e]). Concerning Hen 3-1191, several photometric and spectrometric studies have led to radically different conclusions: the star is reported as a cPNB[e] by Pereira et al. (2003); Zickgraf (2003), a post-AGB object by De Winter & Pérez (1998), a young stellar object (YSO) by De Winter et al. (1994); The et al. (1994), or as a possible symbiotic object (see De Winter et al. 1994). This uncertainty arises from the absence of the major discriminating criteria, the bolometric luminosity – Hen 3-1191's distance is unknown. So, Lamers et al. (1998) fit the star into the ad-hoc group of unclassified objects, unclB[e].

De Winter et al. (1994) started modelling work on Hen 3-1191 and noticed that its spectral energy distribution (SED) in the range 0.4−10 μm could be explained by an early B star photosphere surrounded by dust emitting at a temperature of 950 K. The IRAS measurements from 12 to 100 μm are, however, in excess compared to this model and their slope hints towards the additional presence of a disc or envelope. Elia et al. (2004) successfully used a radiative transfer simulation of Hen 3-1191, with a star surrounded by a spherical CS shell. This model accounts for the SED from 0.4 to 100 μm with the constraint of two polar cavities of relatively small radial extent. No detailed simulation of the spectroscopic data has been carried out so far; studies mainly focus on the presence and width of particular emission lines. Recently, Zickgraf (2003) derived 19 ± 2 km s^{-1} FWHMs for [O I], [N II], Fe II, and [Fe II] lines, and a Hα peak separation of 79 km s^{-1}. No X-ray emission has been detected ($L_X < 7.5\times10^{-16}$ W/m^2) from the star (Hamaguchi et al. 2005).

The advent of optical long-baseline interferometry with spatial resolutions of less than 10 mas and spectral resolutions up to 10 000 allows us, for the first time, to geometrically probe the inner parts of stellar environments. Even with only a few visibility measurements – giving information on the mean spatial

Table 1. Log of Hen 3-1191 MIDI observations. The projected baseline length B_p, the position angle of the base θ_p, and the reduced visibility at the boundaries and the centre of the N band are given. The calibrators used for each observing night are given in the bottom rows of the table.

Night	Time (UT)	B_p(m)	θ_p(°)	$V(8.3\,\mu m)$	$V(10.2\,\mu m)$	$V(12.9\,\mu m)$
2004-04-09[a]	06:53	45.6	33	0.56 ± 0.06	0.51 ± 0.06	0.60 ± 0.06
2004-04-11[b]	05:38	46.3	22	0.45 ± 0.06	0.43 ± 0.06	0.53 ± 0.06
	09:05	41.2	54	0.63 ± 0.06	0.62 ± 0.06	0.70 ± 0.06

[a] Calibrators: HD 107446, 129456, 139127, 152885, 161892, 169916.
[b] Calibrators: HD 81797, 107446, 129456, 139997, 152885, 168723, 176411.

extent – it is possible to disentangle SED models and rule out hypotheses, as shown in recent papers for YSOs (Malbet et al. 1998; Millan-Gabet et al. 2001; Akeson et al. 2002; Lachaume et al. 2003). In particular, the Very Large Telescope Interferometer (VLTI) combined with the N band instrument MIDI gives additional insight in the regions close to stars. See Glindemann et al. (2003) for a recent status report of the VLTI and Leinert et al. (2003) for a description of the MIDI instrument.

In this paper, we present spatially resolved and spectrally dispersed interferometric observations of Hen 3-1191 obtained in the N band (8−13 μm) with VLTI (Sect. 2). In Sect. 3 we use the geometrical information obtained in the previous section and examine three geometrical models that are encountered in both evolved objects and young stellar objects: CS shell, CS disc, and binary. In Sect. 4 we use the models of Sect. 3 and review the four hypotheses on Hen 3-1191's nature.

2. Observation and data reduction

2.1. Photometry and spectroscopic data

The photometric data, presented in Fig. 1, are taken from various sources: JP11 catalogue in the visible, De Winter et al. (1994) and 2Mass in the near-IR, and IRAS in the far-IR. The spectroscopy was obtained as fully reduced and processed data from the Infrared Space Observatory (ISO) archive. Emission features of polyaromatic hydrocarbons (PAHs) are identified at $\lambda\lambda$ 6.2, 7.7, 8.6, and 11.3 μm. There is no noticeable silicate feature at 10 μm. Visible and near-IR data have been dereddened using $A_V = 3$ (It allows us to fit best the visible data with an early star, and is the value reported in the model by Elia et al. 2004).

2.2. Interferometric data

Hen 3-1191 was observed with the UT2-UT3 baseline (length 46.6 m, azimuth 40°) of the VLTI at Cerro Paranal, Chile. Three MIDI visibilities with a spectral resolution of ≈25 in the N band (8−13 μm) were obtained at different hour angles, thus, projected baselines.

The different calibrators observed in the same night predict system visibilities differing by up to ≈0.1 with no clear connection to angular distance from the source or to the time of observation. In order to minimise the risk of systematic errors coming from one calibrator, the system visibility was determined using the average of all calibrators observed on one night. The data reduction was performed with the MIDI Interactive Analysis reduction software (Köhler 2004, incoherent visibility integration in the Fourier space), and we checked that the results were consistent with the results given by the Expert Work Station software (Jaffe 2004, coherent visibility integration in the direct space). The calibrators were also used to derive the spectrum from the uncorrelated fluxes.

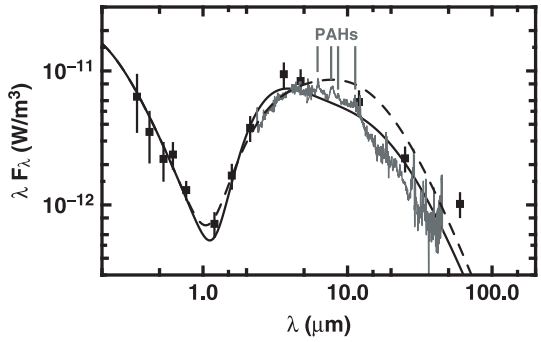

Fig. 1. Observed and modelled SED of Hen 3-1191. *Markers*: photometry. *Gray line*: ISO SWS spectroscopy, *black solid line*: "large gap" model fit, *black dashed line*: "small gap" model fit.

Table 1 sums up the reduced data obtained at three different projected baselines (B_p, θ_p) by giving the calibrated visibility at the centre of the N band and at its boundaries. The detailed spectrum of the visibility is shown in Fig. 4.

Figure 2a displays the uniform disc diameter and their error bars of Hen 3-1191 derived from all observed visibilities. At a given wavelength, the diameter is an average of the ones derived separately for each baseline. The uncertainty includes the scatter of the different diameters and the individual uncertainties on these diameters. The object is clearly resolved with a equivalent uniform disc diameter increasing from 24 ± 3 mas at 8 μm to 36 ± 4 mas at 13 μm. The increase of diameter is steeper from 8 to 10 μm than from 10 to 13 μm, which may arise either from a spectral feature with an excess in size of 10−15% over the continuum represented as a solid line in Fig. 2a, or from a modification in the object's geometry over the band. Not visible in the ISO SWS spectra, a curvature is also weakly seen in the MIDI spectra (both are represented in Fig. 2b).

3. Conditions in the circumstellar environment

The MIDI visibilities unveil a warm CS environment with a uniform disc diameter of 24−36 mas (≈30 AU/kpc). If arising from a flat, wide silicate feature, the 10 μm curvature in these observations would hint towards the presence of micron-sized dust grains (see van Boekel et al. 2005; Kessler-Silacci et al. 2006, for an analysis around HAe/Be stars) at this scale.

In this section, we study the three most common scenarios for a stellar object resolved by means of IR interferometry: a CS disc, a CS envelope, or a binary system made of unresolved components.

3.1. The circumstellar disc scenario

Discs are a common hypothesis around intermediate-mass young stellar objects (Rieke et al. 2005) and evolved stars

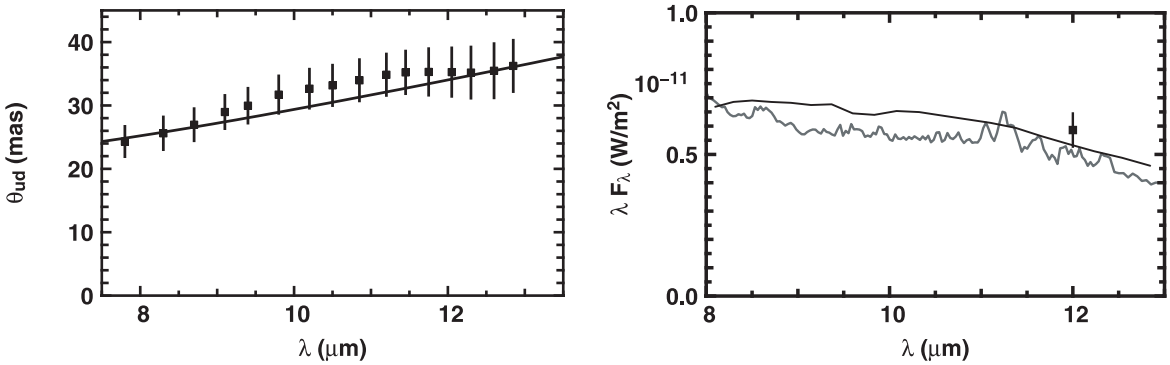

(a) Uniform disc diameter **(b)** MIDI fluxes vs. ISO & IRAS

Fig. 2. Observational date of Hen 3-1191. **b)** MIDI fluxes (black solid line) vs. IRAS 12 μm measurement (square with error bar) and ISO SWS flux (gray solid line). The dashed line also represents an estimated continuum value. **a)** Equivalent uniform disc diameter $\theta_{\rm ud}$ (averaged over baselines) vs. wavelength. The markers and error bars represent values derived from the observation and the dashed line an estimated continuum value.

(Porter 2003). In Herbig HAe/Be stars, the shape of the near-IR excess as well as interferometric observations give constraints on the geometry: the disc features an inner gap beyond the dust sublimation radius, a hot, puffed-up inner rim, directly irradiated by the star (Natta et al. 2001; Dullemond et al. 2001; Monnier et al. 2005). The far-IR excess originates from the remaining parts of the disc, heated by viscous heating and/or stellar light at a grazing angle. A typical sketch of these systems is given by Dullemond et al. (2001, see their Fig. 1).

3.1.1. Model

Our model (see Fig. 3) is a simplification of the aforementioned picture. It uses three flat, infinitely thin elements emitting like black bodies:

- *Star*: disc with temperature $T_\star$ and radius $R_\star$;
- *Inner rim of the disc*: ring of width $h_{\rm r}$, radius $R_{\rm in}$, temperature $T_{\rm r}$, inclination i (0 if pole-on), and position angle θ;
- *Remaining parts of the disc*: disc of inner radius $R_{\rm in}+h_{\rm r}/2$, inclination i, position angle θ, with a radial temperature profile $T(r) = T_{\rm in}(r/R_{\rm in})^{-q}$, where q is a dimensionless parameter ranging from ≈0.5 (irradiated disc) to 0.75 (viscous disc).

The method to compute the spectra and visibilities from these geometrical elements is based on the Hankel transform (disc) or analytical expressions (star and ring). Further details are available in Malbet et al. (2005).

In order to obtain a physically relevant model, we self-consistently determine the location of the inner rim $R_{\rm in}$ as a function of stellar luminosity by assuming that it is located where the dust sublimates. The "small gap scenario" proposed for luminous stars ($\gtrsim 10^3\,L_\odot$) by Monnier et al. (2005) states that there is enough gas in the sublimation region to shadow the disc from the star. Then, the inner rim is heated by irradiation at a grazing angle from above the surface of the disc. From Fig. 4 in Monnier et al. (2005), we derived

$$R_{\rm in} = 7.0\times10^{-2}\left(\frac{T_\star}{T_\odot}\right)^{1.6}\left(\frac{T_{\rm r}}{1000\,{\rm K}}\right)^{-1.2}\left(\frac{R_\star}{1\,R_\odot}\right)^{0.8}\ {\rm AU}, \qquad (1)$$

where $T_\star$ and $R_\star$ are the effective temperature and radius of the star, and $T_{\rm r}$ the temperature of the inner rim. The "large gap scenario", as explained by Dullemond et al. (2001); Monnier et al. (2005) states that the rim is indeed directly heated by the star

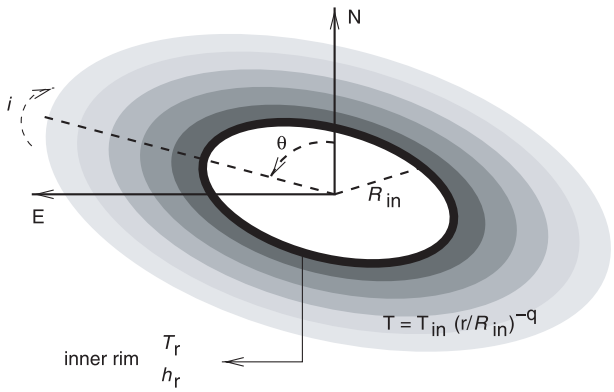

Fig. 3. Sketch of an optically thick CS disc around an intermediate-mass star. It consists of a flat disc with an inner irradiated rim.

because the inner region is gas-free or only contains optically thin gas. Then,

$$R_{\rm in} = 0.24\,(2\epsilon)^{-0.5}\left(\frac{R_\star}{R_\odot}\right)\left(\frac{T_\star}{T_\odot}\right)^{2}\left(\frac{T_{\rm r}}{1000\,{\rm K}}\right)^{-2}\ {\rm AU}, \qquad (2)$$

where ϵ is the ratio of the ring opacity for its own radiation to its opacity for the stellar radiation (as in Chiang & Goldreich 1997).

3.1.2. Results

We derived best-fit models of the photometric, spectroscopic, and interferometric data. Due to the large numbers of ISO data (35 000 points) compared to photometry and visibilities (a few tens), a standard least-square fitting procedure would only give weight to the spectroscopy. Therefore, we computed separated reduced chi squares for the three kind of observables, respectively $\chi^2_{\rm ph.}$, $\chi^2_{\rm sp.}$, and $\chi^2_{\rm vis}$, and minimised their average $\chi^2_{\rm tot}$. Combined with the presence of large, systematic calibration errors that the standard least-squares method does not handle, this algorithm prevents us from obtaining reliable uncertainties on derived parameters; our estimates were derived from the geometrical mean of the uncertainties given by the photometric and interferometric chi squares.

We achieved a satisfactory agreement between the "large gap" model and data, but we were not able to do so for the "small gap" hypothesis. In the latter case, we only minimised using $\chi^2_{\rm ph.}$ and $\chi^2_{\rm vis}$; the resulting fit is clearly not consistent with the

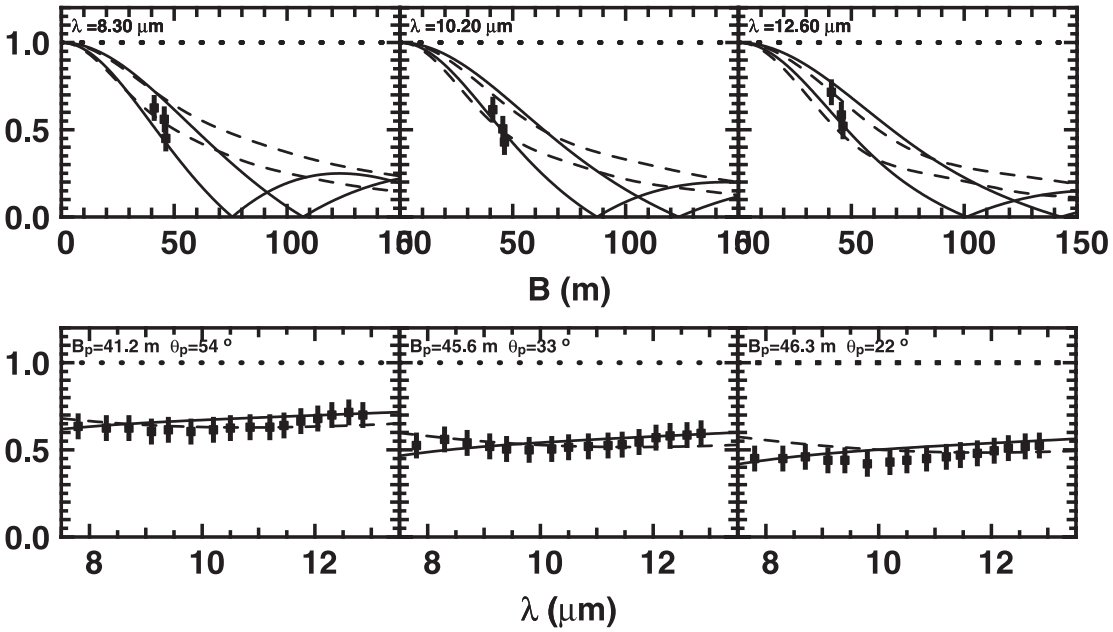

Fig. 4. Observed and modelled visibilities of Hen 3-1191. *Markers*: MIDI visibilities *Black solid line*: "large gap" model fit to the SED and visibilities. *Black dashed line*: "small gap" model fit of the SED and visibilities. *Top panel*: visibility vs. baseline at the boundaries and in the centre of the N band. The visibility curve along the major axis (lower curve of a pair) and the minor axis (upper curve of a pair) of the inclined disc are given. *Bottom panel*: visibility vs. wavelength for each of the three baselines.

Table 2. Best-fit model of Hen 3-1191 visibilities and SED with a parametrised disc model. Figures appear in pairs, the left one stands for the "large gap" (lg) model, the right one for the "small gap" (sg) model.

	lg	sg		lg	sg
d (kpc)[a]	4	4	$R_\star$ ($R_\odot$)	6.0 ± 0.3	6.0 ± 0.5
$T_\star$ (K)[a]	25 000	25 000	ϵ	0.30 ± 0.08	–
i (°)	45 ± 10	45 ± 8	θ (°)	0 ± 3	1 ± 4
q	0.76 ± 0.02	0.50 ± 0.03	$T_{\rm in}$ (K)	510 ± 60	1640 ± 150
$h_{\rm r}$ (AU)	2.4 ± 0.2	1.2 ± 1.0	$T_{\rm r}$ (K)	1080 ± 90	1000 ± 110
$R_{\rm in}$ (AU)	30 ± 2	2.3 ± 0.2	$R_{\rm out}$ (AU)[a]	150	150
$\chi^2_{\rm ph.}$	2.62	3.37	$\chi^2_{\rm sp.}$	2.59	12.31
$\chi^2_{\rm vis}$	0.56	0.72	$\chi^2_{\rm tot}$	1.91	5.46

[a] Value assumed and kept constant.

spectroscopy ($\chi^2_{\rm sp.} = 12.3$). The model parameters and chi squares are given in Table 2. The comparison between model and data are displayed in Figs. 1 and 4.

First, the "large gap" model fits the data better than the "small gap" model – only marginally for visibilities, but substantially for photometry and spectroscopy. Second, the small gap models leads to physically inconsistent parameters: the temperature law features $q = 0.50$ hinting towards a flared, irradiated disc while the inner temperature of the disc at the inner rim $T_{\rm in} \approx 1640$ K is much too large for irradiation. Since the small gap model implies that matter beyond radius $R_{\rm in}$ is irradiated at a grazing angle like the remaining parts of the disc, we should have $T_{\rm in} = T_{\rm r} \approx 1000$ K, which is a factor of 7.5 below in terms of flux. We therefore conclude that, provided that the disc scenario is correct, Hen 3-1191 features a wide gap (30 AU) almost free of matter or consisting of optically thin gas.

The wide gap models hints towards an active disc (temperature law with $q = 0.76$), which is valid for both an accretion disc (Shakura & Sunyaev 1973) or an excretion disc (Lee et al. 1991). From the disc temperature ($T_{\rm in} = 510$ K) at the inner rim (30 AU) we can derive the accretion or excretion rate $\dot{M}$ from the standard laws for each of these discs. Substituting $R = R_{\rm in} \gg R_\star$, $R_0 = R_\star$, and $Q = \sigma T_{\rm in}^4$ in the first and fourth terms of Eq. (2.6) by Shakura & Sunyaev (1973) we obtain the accretion rate

$$\dot{M} = \frac{8\pi\sigma T_{\rm in}^4 R_{\rm in}^3}{3GM_\star} \tag{3a}$$

$$\approx 2.5\times10^{-2}\left(\frac{M_\star}{14\,M_\odot}\right)^{-1}\left(\frac{d}{4\,\rm kpc}\right)^{3} M_\odot/\rm yr \tag{3b}$$

where d is the distance to the star if we apply a distance scaling to $R_{\rm in}$ in our model computed for a distance of 4 kpc. For an excretion disc, we carry out the substitutions $\Omega^2 = GM_\star/R_{\rm in}^3$, $Q^+_{\rm vis} = 2\sigma T_{\rm in}^4$, $r = R_{\rm in}$, $r_1 = R_{\rm out} \gg R_{\rm in}$ in Eq. (12) by Lee et al. (1991) and find

$$\dot{M} = \frac{8\pi\sigma T_{\rm in}^4 R_{\rm in}^{7/2}}{3GM_\star R_{\rm out}^{1/2}} \tag{4a}$$

$$\approx 4.3\times10^{-3}\left(\frac{M_\star}{14\,M_\odot}\right)^{-1}\left(\frac{R_{\rm out}}{1000\,\rm AU}\right)^{-1/2}\left(\frac{d}{4\,\rm kpc}\right)^{7/2} M_\odot/\rm yr, \tag{4b}$$

where $R_{\rm out}$ is the outer radius of the excretion disc.

3.2. The circumstellar shell scenario

3.2.1. Model

Elia et al. (2004) successfully explained the SED of Hen 3-1191 with a CS shell without polar holes – but polar cavities of small radial extension. Since the star features a large-scale bipolar nebula (De Winter et al. 1994), probably resulting from an outflow, we conversely assume the shell should feature polar holes. The sketch of such a model is represented in Fig. 5. Furthermore, the star is likely to be seen through this hole, since the moderate

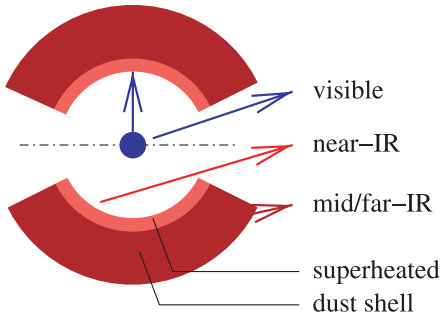

Fig. 5. Sketch of the CS shell. Arrows represent light beams.

Table 3. Parameters of the envelope model. Instead of the density at the inner rim used in the model, the optical thickness in the visible is given.

$L_\star$	$1.26 \times 10^3\ L_\odot$
τ_V	0.5
θ_0	30 °
q	0.5
$T_{\rm sub}$	1000 K

extinction ($A_V \lesssim 3$, see Elia et al. 2004, Table 2) is probably interstellar, placing the star at the distance of 4−5 kpc (assuming an early B main-sequence star) in the galactic plane.

We used the iterative numerical radiative transfer simulation described in Sonnhalter et al. (1995) in order to derive the temperature distribution around the star from a fixed, assumed density distribution. Once convergence of radiation field and temperature are achieved, ray-tracing is performed to obtain images and fluxes from the density and temperature distribution. The space within the self-consistently determined sublimation radius is assumed free of matter, as are the conic polar holes. The simulation uses the flux-limited diffusion approximation (Levermore & Pomraning 1981) in a set of concentric square meshes. The 2D distribution in the (r, θ) space is written

$$\rho(r,\theta) = \begin{cases} \rho_0 (r/r_0)^{-q} & \text{if } r > r_0 \text{ and } \theta < \theta_0 \\ \epsilon\rho_0 (r/r_0)^{-q} & \text{if } r > r_0 \text{ and } \theta > \theta_0 \\ 0 & \text{if } r < r_0 \end{cases} \quad (5)$$

where θ_0 is the opening angle of the polar holes, ρ_0 and r_0 the density and location of the sublimation radius, q the density exponent, and $\epsilon = 10^{-4}$ a small factor used to prevent numerical instabilities.

3.2.2. Results

We tried to fit SED and visibilities using the envelope model but we failed to find a model consistent with the observations. Table 3 lists the parameters of an envelope model that fits the SED (see Fig. 6, left panel), but all models give too large structures (by a factor of at least two) in order to explain the MIDI observations (e.g. same figure, right panel). The optical thickness we derive from the SED is different from the one found by Elia et al. (2004, $\tau_V = 2.7$) but the density distribution follows the same power law ($q = 0.5$). The discrepancy may arise from different opacity laws in our model ($\kappa_\lambda \propto 2$ in the submillimeter) and theirs ($\kappa_\lambda \propto \lambda^{-1.2}$), or from the difference in the CS geometry (our models involves a sublimation cavity free of matter while these authors assume it contains gas).

We can explain the difficulty to find a consistent fit of visibilities with an envelope by comparing it with a disc: the envelope occupies a larger solid angle than the inner disc rim, so that the envelope has to be optically thin in order to reprocess the same amount of stellar light and feature a similar IR excess. Then, it means that light is absorbed further out in the envelope and that the corresponding uniform disc diameter is larger.

3.3. The binary scenario

Since the mid-IR flux is in excess by a factor of 100 compared to that of the stellar photosphere, a binary system that accounts for the N-band visibilities must consist of two objects featuring a large IR flux, thus a large amount of CS dust. Such a picture is complex, for it involves possibly resolved components, and the few geometrical data available could not constrain such a model. We therefore consider a simplistic approach using two unresolved components; however, we can expect that the flux ratio strongly varies with wavelength since the SED of IR sources exhibit a large variety of behaviours: for instance, a companion featuring a flat SED around a companion with a standard accretion disc has a flux ratio going as $F_\lambda \propto \lambda^{5/3}$ (Shakura & Sunyaev 1973, $F_\nu \propto \nu^{1/3}$ in their disc model).

We decided not to try to explain the SED with this model, since it would require detailed knowledge of the components. Instead, we use an ad hoc binary model made of two point-like sources with linear separation r, position angle θ, and wavelength-dependent flux ratio

$$f = f_0 \left(\frac{\lambda}{\lambda_0}\right)^s, \quad (6)$$

where f_0 is the flux ratio at the reference wavelength λ_0, and s an exponent.

We found several binary models that fit the MIDI visibilities well, so that the binary scenario cannot be a priori excluded. We present the model fits with the least separation, around 18 AU per kpc of distance. Its parameters are given in Table 4 and the fit of MIDI visibilities is displayed in Fig. 7.

4. Nature of the object

4.1. The supergiant hypothesis

B[e] supergiants with an effective temperature hotter than 20 000 K – that of Hen 3-1191 is around 30 000 K – have a bolometric luminosity greater than $10^5\ L_\odot$ (Lamers et al. 1998, see their Fig. 1), that is an absolute bolometric magnitude brighter than −7.8. For a B0-B1 star, the bolometric correction is as small as −2.8 (see the catalogue by Bessell et al. 1998), so the absolute visual magnitude is brighter than −5.0. Having a dereddened magnitude $V \approx 10$, Hen 3-1191 should be placed at a distance of at least 10 kpc. Since it is at a small galactic longitude in the plane of the galaxy, one would expect an interstellar visual extinction of the order of $10^{\rm m}$, which is clearly not the case ($A_V \lesssim 3$, see Elia et al. 2004, Table 2). Therefore, we deem that Hen 3-1191 does not belong to the sgB[e] class.

4.2. The Herbig Ae/Be hypothesis

We were able to model Hen 3-1191 with a parametric disc model featuring the properties often encountered in Herbig Ae/Be stars: an inner rim at the sublimation temperature accounting for the 1−5 μm flux and the remaining, cooler parts of the disc that dominate the 10−100 μm SED. However, the properties of the YSO in this scenario are rather unusual and contradictory.

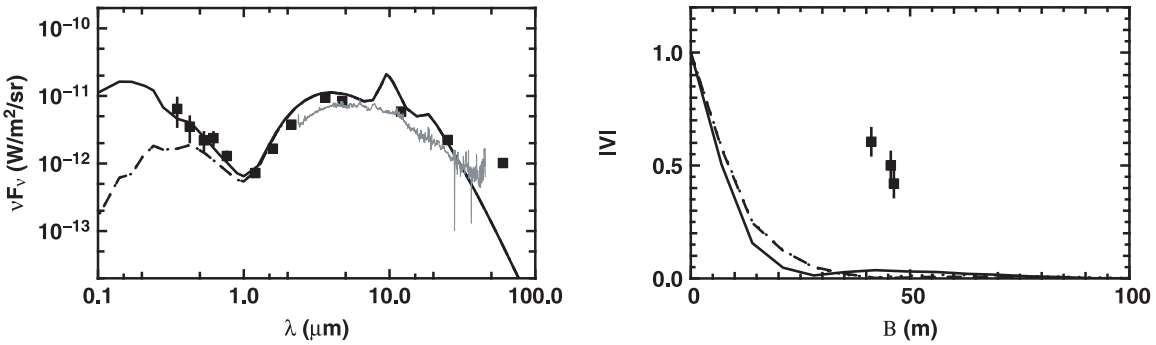

Fig. 6. SED and visibilities of Hen 3-1191: model fit using the spherical shell model with polar holes. *Solid line*: pole-on model. *Dashed line:* equator-on model. *Left:* SED. *Right*: visibilities vs. baseline

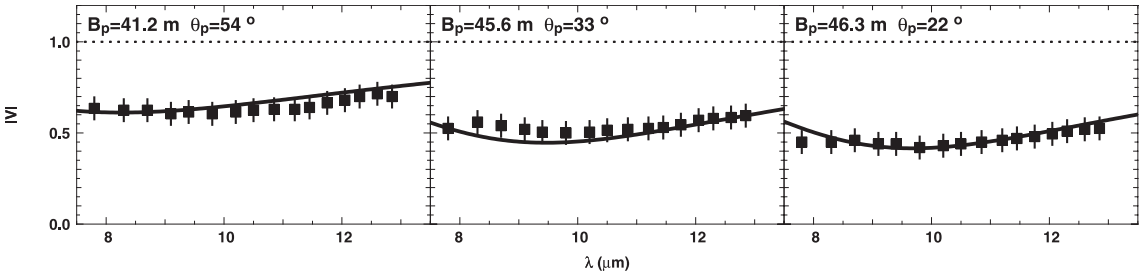

Fig. 7. Binary model fit: visibility vs. wavelength at each spatial frequency probed by MIDI. Line: model; markers with error bars: MIDI data.

Table 4. Parameters of a binary model fit to the MIDI visibilities.

distance	d	4 kpc[a]
separation	r	71 AU
position angle	θ	70°
flux ratio	f_0 at $\lambda_0 = 10\,\mu$m	0.55
flux ratio slope	s	2.28

[a] Assumed value.

First, the disc features a large (30 AU in radius), almost free-of-matter ("wide gap scenario") inner gap, whereas it undergoes a short-lived phase of unusually high mass accretion: the mass flow is $\dot{M} \sim 4$–$250 \times 10^{-4}\ M_\odot$/yr, depending on accurate distance – we "liberally" assume from 1 to 4 kpc. It lies above the typical one in FU Ori outbursts (Hartmann & Kenyon 1996). If such an accretion rate is correct, we conversely expect the inner gap to be filled with optically thick gas ("small gap scenario").

If we further follow the common HAe/Be picture, the Hα line originates from rotating material, so that the peak-to-peak of $\approx$70 km s^{-1} separation measured by Zickgraf (2003) implies material rotating at $\approx 35/\sin i$ km s^{-1} around the star. With a typical young early B star mass of 10–15 $M_\odot$, the material must be located within 5 AU from the star, once again pointing towards the "small gap scenario".

Lastly, the P Cygni profiles characteristic of HAe/Be stars are absent in the spectrum of Hen 3-1191.

Considering the previous points, the Herbig Ae/Be disc scenario is therefore unlikely, though we cannot completely rule it out. An alternative explanation is that the mid and far-IR excess is not to be imputed to a strongly accreting disc only, but to the presence of an envelope or wind in addition to a disc. This scenario would allow smaller accretion rates and be consistent with absent P Cygni profiles and the absence of gas in the inner gap of the disc; it would not require that we observe an unlikely outburst. However, this alternative scenario requires more elaborate modelling that we have not performed yet.

4.3. The protoplanetary nebula hypothesis

The large-scale (4″) bipolar nebula observed in the optical by De Winter et al. (1994) as well as the similarity of its spectrum to that of the Luminous Blue Variable η Car and those of some confirmed proto-PNs (le Bertre et al. 1989) are strong arguments in support of this hypothesis. We note, however, that the IRAS colours of Hen 3-1191 do not fit well within characteristics of post-AGB objects given by Kwok (1993); van der Veen & Habing (1988), as shown in Fig. 8 (region VIa, mostly made of unidentified Be or variable stars).

The absence of high excitation lines (Landaberry et al. 2001, e.g. [O III] [N III]) as well as the hot ($\approx$1000 K) mid-IR temperature hints towards a dense, compact, and young post-AGB object. Moreover, the linear size of the CS material obtained with our MIDI measurements is

$$r \approx 30 \left(\frac{d}{1\,\mathrm{kpc}} \right) \mathrm{AU}, \tag{7}$$

where d is the distance to the object. With an upper limit around 5 kpc from the relatively low extinction, this places the hot material at a distance of at most 150 AU from the central star, which indicates that the mass loss is recent or still ongoing.

There is strong evidence that proto-PNs feature either a disc-like environment or a highly asymmetrical shell with a wide polar cone containing optically thin or moderately optically thick material (Kwok 1993; Zickgraf 2003). Our model of Sect. 3.1 yields an equatorial mass loss rate $\dot{M} \gtrsim 4 \times 10^{-5}\ M_\odot$/yr using $M_\star \leq 8\,M_\odot$ (maximum mass of proto-PNs after Kastner 2005), $R_{\mathrm{out}} \leq 2500$ AU (value observed in another object by Kwok et al. 2000, a likely upper limit for a young proto-PN), and a conservative distance estimate ($d \geq 1$ kpc). This is of the order of magnitude of the total (i.e. equatorial and bipolar) mass loss rates modelled from proto-PN observations by Hrivnak & Bieging (2005). However, the values specifically modelled in excretion discs around other types of Be stars differ by several orders of magnitude (from $\ll 10^{-9}$ to $>2.5 \times 10^{-5}\ M_\odot$/yr cited by

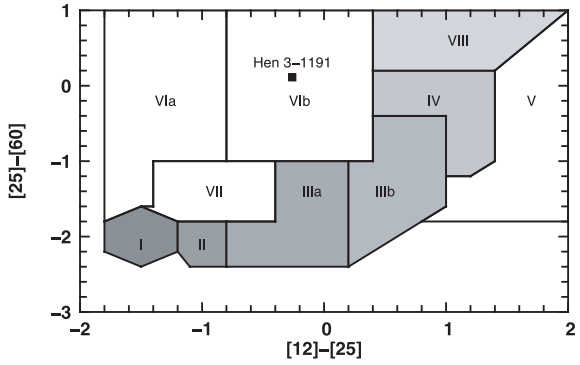

Fig. 8. Position of Hen 3-1191 in the IRAS colour-colour diagram and comparison with the classification by van der Veen & Habing (1988). Shaded regions indicate the evolutionary track of post-AGB objects. (Zero magnitude at 1 Jy in all bands.)

Lee et al. 1991; Okazaki 2001; Kraus et al. 2007), so that we cannot draw a conclusion concerning the validity of our mass loss rate.

4.4. The symbiotic star hypothesis

Our binary model, with a small separation of at least ≈18 AU per kpc of distance does not fit well with the accepted picture of symbiotic stars (Kenyon & Webbink 1984): a hot companion accreting material from a very close late-type companion. In addition, the characteristic size of the CS dust in most symbiotic stars – except those with a Mira star – is reported to be of the order of 1 AU by Leedjärv (2006), while the uniform disc diameter of Hen 3-1191 is ≈30 AU per kpc of distance.

Furthermore, Hen 3-1191 does not show evidence of the presence of a late-type companion (absence of TiO lines according to Landaberry et al. 2001) and no high ionisation lines ([O III] & [N III], same authors), that are standard characteristics of dusty symbiotic stars. Furthermore this scenario requires a large variability (>1 mag in the *J* band) in the near-IR as measured in such symbiotic stars by Feast et al. (1977). On the contrary, le Bertre et al. (1989) measured little variability (<0.1 mag over the near-IR).

We therefore conclude that Hen 3-1191 is not a symB[e].

5. Conclusion

We observed and resolved the innermost parts of the CS matter around the B[e] star Hen 3-1191 using MIDI on the VLTI, yielding a uniform disc diameter of 24 to 36 mas over the N band. Together with the SED, these observations can be explained with a CS disc featuring a wide inner gap and an unusually high accretion or excretion, whereas an envelope is not able to account for them. A binary system made of two unresolved IR sources with different SED slopes in the IR may also account for the MIDI visibilities; we did not investigate this hypothesis in detail, since the available data only puts very loose constraints on such a system.

However, these observations do not allow us to give a definitive answer about the nature of the object. The supergiant and symbiotic star scenarios are extremely unlikely, so that Hen 3-1191 is most likely a young, compact proto-PN or a Herbig Be star. However, in the Herbig HAe/Be scenario, the model parameters reveal an atypical nature, though the additional presence of an envelope or wind could explain part of the strong mid-IR flux.

Additional observations are required to determine the true nature of Hen 3-1191. Wide field imaging may reveal a nearby star forming region; diffraction-limited observations in the optical may also reveal bipolar nebular structure characteristic of PNs; high resolution spectroscopy may also be a key to the chemistry of the object, thus its evolutionary stage. Additional observations at the VLTI, in the near and mid-IR with AMBER and MIDI will also be of use to obtain better constraints on the geometry of the CS matter and to confirm or invalidate the accretion disc scenario with or without the envelope, or binarity.

Acknowledgements. This work has made use of NASA's Astrophysics Data System. It also made use of the SIMBAD database and Vizier catalogue access tool, both operated at CDS, Strasbourg, France. Most computations and graphics have been made with the free software Yorick developed by David H. Munro. We thank the anonymous referee for a constructive report which helped to improve the quality of this paper.

References

Akeson, R. L., Ciardi, D. R., van Belle, G. T., & Creech-Eakman, M. J. 2002, ApJ, 566, 1124
Allen, D. A., & Swings, J. P. 1972, Astrophys. Lett., 10, 83
Allen, D. A., & Swings, J. P. 1976, A&A, 47, 293
Bessell, M. S., Castelli, F., & Plez, B. 1998, A&A, 333, 231
Chiang, E. I., & Goldreich, P. 1997, ApJ, 490, 368
De Winter, D., & Pérez, M. R. 1998, in B[e] stars, ASSL, 233, 269
De Winter, D., The, P. S., & Perez, M. R. 1994, in Astron. Soc. Pacific Conf. Ser., 413
Dullemond, C. P., Dominik, C., & Natta, A. 2001, ApJ, 560, 957
Elia, D., Strafella, F., Campeggio, L., et al. 2004, ApJ, 601, 1000
Feast, M. W., Robertson, B. S. C., & Catchpole, R. M. 1977, MNRAS, 179, 499
Glindemann, A., Algomedo, J., Amestica, R., et al. 2003, Ap&SS, 286, 35
Hamaguchi, K., Yamauchi, S., & Koyama, K. 2005, ApJ, 618, 360
Hartmann, L., & Kenyon, S. J. 1996, ARA&A, 34, 207
Hrivnak, B. J., & Bieging, J. H. 2005, ApJ, 624, 331
Jaffe, W. J. 2004, in New Frontiers in Stellar Interferometry, Proc. SPIE, ed. W. A. Traub (Bellingham, WA: The International Society for Optical Engineering), 5491, 715
Kastner, J. H. 2005, in BAAS, 469
Kenyon, S. J., & Webbink, R. F. 1984, ApJ, 279, 252
Kessler-Silacci, J., Augereau, J.-C., Dullemond, C. P., et al. 2006, ApJ, 639, 275
Köhler, R. R. 2004, in E-cookbook of the MIDI data reduction, analysis and science workshop, `http://www.strw.leidenuniv.nl/~nevec/workshop_2004/e_cookbook/MIA/index.html`
Kraus, M., Borges Fernandes, M., & de Araújo, F. X. 2007, A&A, 463, 627
Kwok, S. 1993, ARA&A, 31, 63
Kwok, S., Hrivnak, B. J., & Su, K. Y. L. 2000, ApJ, 544, L149
Lachaume, R., Malbet, F., & Monin, J.-L. 2003, A&A, 400, 185
Lamers, H. J. G. L. M., Zickgraf, F., De Winter, D., Houziaux, L., & Zorec, J. 1998, A&A, 340, 117
Landaberry, S. J. C., Pereira, C. B., & de Araújo, F. X. 2001, A&A, 376, 917
le Bertre, T., Epchtein, N., Gouiffes, C., Heydari-Malayeri, M., & Perrier, C. 1989, A&A, 225, 417
Lee, U., Osaki, Y., & Saio, H. 1991, MNRAS, 250, 432
Leedjärv, L. 2006, Ap&SS, 304, 105
Leinert, C., Graser, U., Przygodda, F., et al. 2003, Ap&SS, 286, 73
Levermore, C. D., & Pomraning, G. C. 1981, ApJ, 248, 321
Malbet, F., Berger, J.-P., Colavita, M. M., et al. 1998, ApJ, 507, 149
Malbet, F., Lachaume, R., Berger, J.-P., et al. 2005, A&A, 437, 627
Millan-Gabet, R., Schloerb, F. P., & Traub, W. A. 2001, ApJ, 546, 358
Monnier, J. D., Millan-Gabet, R., Billmeier, R., et al. 2005, ApJ, 624, 832
Natta, A., Prusti, T., Neri, R., et al. 2001, A&A, 371, 186
Okazaki, A. T. 2001, PASJ, 53, 119
Pereira, C. B., Landaberry, S. J. C., & de Araújo, F. X. 2003, A&A, 402, 693
Porter, J. M. 2003, A&A, 398, 631
Rieke, G. H., Su, K. Y. L., Stansberry, J. A., et al. 2005, ApJ, 620, 1010
Shakura, N. I., & Sunyaev, R. A. 1973, A&A, 24, 337
Sonnhalter, C., Preibisch, T., & Yorke, H. W. 1995, A&A, 299, 545
The, P. S., De Winter, D., & Perez, M. R. 1994, A&AS, 104, 315
van Boekel, R., Min, M., Waters, L. B. F. M., et al. 2005, A&A, 437, 189
van der Veen, W. E. C. J., & Habing, H. J. 1988, A&A, 194, 125
Zickgraf, F.-J. 1998, in B[e] stars, ASSL, 233, 1
Zickgraf, F.-J. 2003, A&A, 408, 257